Resonant and Phonon-Assisted Excitation Energy Transfer within the R_1 Lines of $[Cr(Ox)_3]^{3-}$ in a System with Two Crystallographically Non-equivalent Lattice Sites

Marianne E. von Arx and Andreas Hauser*

Département de chimie physique, Université de Genève, 30, quai Ernest-Ansermet CH-1211 Geneva 4, Switzerland

Received: January 17, 2002

The $[Ru(bpy)_3][LiCr(ox)_3]$ system (bpy = 2,2′-bipyridine, ox = oxalate) has two crystallographically non-equivalent $[Cr(ox)_3]^{3-}$ sites. In steady-state resonant and nonresonant fluorescence line narrowing (FLN) experiments on the R_1 lines of the two non-equivalent $[Cr(ox)_3]^{3-}$ chromophores, multiline spectra are observed at 1.6 K. Such multiline spectra are clear evidence for resonant energy transfer processes within the inhomogeneously broadened R_1 lines. In addition, time-resolved experiments show that also site-to-site energy transfer occurs, which turns out to be resonant, too, however with a non-negligible phonon-assisted contribution even at 1.5 K.

1. Introduction

Recently, we reported on the excitation energy transfer properties of $[Cr(ox)_3]^{3-}$ chromophores in the three-dimensional network structure $[Rh(bpy)_3][NaCr(ox)_3]ClO_4$ (ox = oxalate, bpy = 2,2′-bipyridine).[1,2] At 1.8 K, energy migration within the electronic origin of the low-energy component of the ^2E state, the so-called R_1 line, was found to be an efficient resonant process. This was in fact, the first system for which efficient energy migration with clearly resonant character has been reported. Otherwise, excitation energy transfer between identical chromophores, in particular energy migration in Cr^{3+} doped systems such as ruby, was found to be dominated by phonon-assisted processes, with at most a very small resonant contribution.[3−10]

The present paper reports on an investigation of resonant and phonon-assisted energy transfer in $[Ru(bpy)_3][LiCr(ox)_3]$. At room temperature this system crystallizes in the cubic space group $P2_13$,[11] with the $[Cr(ox)_3]^{3-}$ units having C_3 point symmetry. Each oxalate ion acts as bridging ligand between Cr^{3+} and Li^+. The $[LiCr(ox)_3]^{2-}$ units thus form a tree-dimensional negatively charged network. The charge compensating $[Ru(bpy)_3]^{2+}$ cations occupy the cavities provided by the network structure. The basic spectroscopic behavior of Cr^{3+} in this system is identical to that of the large number of octahedrally coordinated and trigonally distorted Cr^{3+} chromophores studied to date [12,13] as well as to the $[Rh(bpy)_3][NaCr(ox)_3]ClO_4$ system mentioned above.[1] However, low-temperature absorption and luminescence measurements show that in $[Ru(bpy)_3][LiCr(ox)_3]$ the $[Cr(ox)_3]^{3-}$ units sit on two crystallographically non-equivalent lattice sites. Taking this into account, energy transfer processes between the chromophores on one site as well as site-to-site energy transfer processes are to be expected. Steady-state and time-resolved fluorescence line narrowing (FLN) as well as excitation line narrowing (ELN) measurements are employed to distinguish between the different processes. The previously discussed model for resonant energy transfer in a one-site system[1] is applied and extended to explain the resonant energy transfer processes in this two-site system.

2. Experimental Section

$[Ru(bpy)_3][LiCr(ox)_3]$ was prepared as described in refs 14 and 15. Spectroscopic measurements were generally performed on polycrystalline samples. Only the absorption spectrum of $[Ru(bpy)_3][LiCr(ox)_3]$ was recorded on a single crystal in the form of a perfect tetrahedron (1 μm edge) with one corner polished off.

Steady-state and time-resolved fluorescence line narrowing and broad band excitation spectra were performed on the setup described in ref 16. For time-resolved measurements, a photoelastic modulator (Automates et Automatismes MT0808) was used in addition to the mechanical chopper in order to produce laser pulses of 1−4 μs. The time-resolved luminescence was recorded using the gated photon counting system at fixed delays for full spectra. For excitation line narrowing spectra the Ti:sapphire ring laser was scanned by a stepper motor with a gearing ratio of 0.0013 nm (0.027 cm^{-1}) per step in the region of 690−700 nm, and the luminescence was detected resonantly at the wavelength of the R_1 line using a double monochromator (Spex 1404) and slit widths of 20 μm, (spectral resolution ∼0.3 cm^{-1}).

3. Results

3.1. Luminescence and Absorption Spectra. The absorption spectrum of the $[Cr(ox)_3]^{3-}$ chromophore in $[Ru(bpy)_3][LiCr(ox)_3]$ is expected to show a similar behavior as generally found for trigonally distorted $[Cr(ox)_3]^{3-}$ in other matrices.[1,13,14,16] In particular, the $^4A_2 \rightarrow {}^2E$ spin-flip transition is expected to be the lowest-energy transition. In three-dimensional oxalato networks, it is easily identified as a doublet of sharp lines at around 14400 cm^{-1}, with a zero-field splitting between 12 and 18 cm^{-1}.[1,14,16−18]

The absorption spectrum in the region of the $^4A_2 \rightarrow {}^2E$ transitions (R lines) of $[Ru(bpy)_3][LiCr(ox)_3]$ at 10 K is shown in Figure 1. Instead of the expected two lines due to the zero-field splitting of the ^2E state, it consists of three lines: one

* Corresponding author. Fax: (++41) (0)22 702 6103. E-mail: Andreas.Hauser@chiphy.unige.ch

10.1021/jp020174y CCC: $22.00
Published on Web 07/12/2002

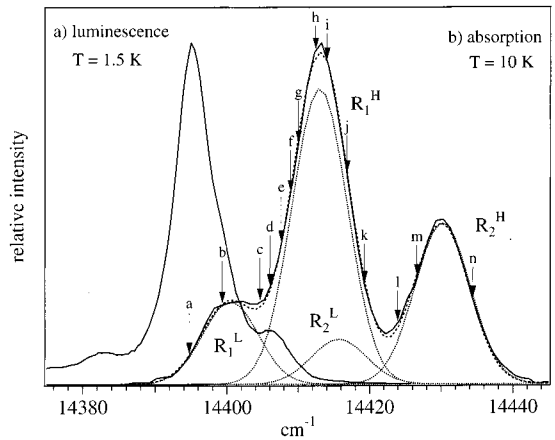

Figure 1. (a) Luminescence spectrum in the region of the R lines of $[Ru(bpy)_3][LiCr(ox)_3]$ at 1.5 K upon excitation into the $^4A_2 \rightarrow {}^4T_2$ transition at 482 nm. (b) Absorption spectrum in the region of the R lines of $[Ru(bpy)_3][LiCr(ox)_3]$ at 10 K. Fit to the absorption spectrum as described in the text (- - -), and decomposition into the four Gaussians (····). The arrows mark the frequencies of the narrow band laser excitation for the FLN experiments of Figure 2.

dominant line at 14413.0 cm^{-1} flanked by a line of lesser intensity at 14430.2 cm^{-1} and a third line on the low energy side at approximately 14400 cm^{-1}. This indicates that there are at least two crystallographically non-equivalent sites available for Cr^{3+}, having slightly different excited-state energies. In the following the high-energy site is called "site H", the low-energy site "site L". Thus, the line with the maximum at 14430.2 cm^{-1} corresponds to the R_2^H line, the line with the maximum at 14413.0 cm^{-1} is a superposition of the R_1^H and R_2^L lines, and the low energy shoulder is assigned to the R_1^L line.

Upon excitation at 18416 cm^{-1} (543 nm), that is into the $^4T_2$ absorption band of the $[Cr(ox)_3]^{3-}$ chromophore in $[Ru(bpy)_3][LiCr(ox)_3]$, sharp line luminescence assigned to the $^2E \rightarrow {}^4A_2$ transition is observed. Figure 1 includes the corresponding luminescence spectrum at 1.5 K in the region of the R lines. It consists of a single line with its maximum at 14395.1 cm^{-1} and a full width at half-maximum (fwhm) of 7.5 cm^{-1}. Two small shoulders can be seen at either side of the prominent line. A broad background luminescence is additionally observed at the low energy side. The fact that luminescence at 1.5 K is observed predominantly from R_1^L indicates that there is efficient site-to-site energy transfer.

3.2. Fluorescence Line Narrowing (FLN). The zero-field splittings of the $^4A_2$ ground state of the two sites D^H and D^L are smaller than the inhomogeneous line widths Γ_{inh} and are not resolved in the spectra of Figure 1. In the absence of energy migration such zero-field splittings can nevertheless be resolved using the technique of fluorescence line narrowing (FLN)[19,20] with narrow band laser excitation tuned to the R_1 line of the Cr^{3+} chromophore. The resulting FLN spectrum characteristically consists of three lines: the central or resonant line at the excitation frequency and satellites at $\pm D$.[1,3,19,21] The relative intensities of the three lines depend on the sample temperature, on the relative transition probabilities of the two transitions, on the ratio of the width of the inhomogeneous distribution to the value of D, and on the excitation frequency within the inhomogeneous distribution.

In concentrated systems, excitation energy transfer within the R_1 line of the $^4A_2 \rightarrow {}^2E$ transition is a common phenomenon.[22] In an FLN experiment, strongly temperature dependent phonon-assisted energy transfer results in spectral diffusion into the inhomogeneously broadened band.[22] Energy selective resonant energy transfer, on the other hand, results in characteristic multiline patterns.[1] Except at very low temperature, the former is usually dominant.

Figure 2 shows the luminescence spectra of $[Ru(bpy)_3][LiCr(ox)_3]$ at 1.6 K for selective excitation within the R lines of the $[Cr(ox)_3]^{3-}$ chromophore. Very different FLN spectra are obtained depending on the exact excitation frequency. Resonant FLN spectra of the R_1^L line show multiline patterns at 1.6 K (Figure 2, spectra a−d). The number and the intensities of the individual lines depend critically on the excitation frequency.

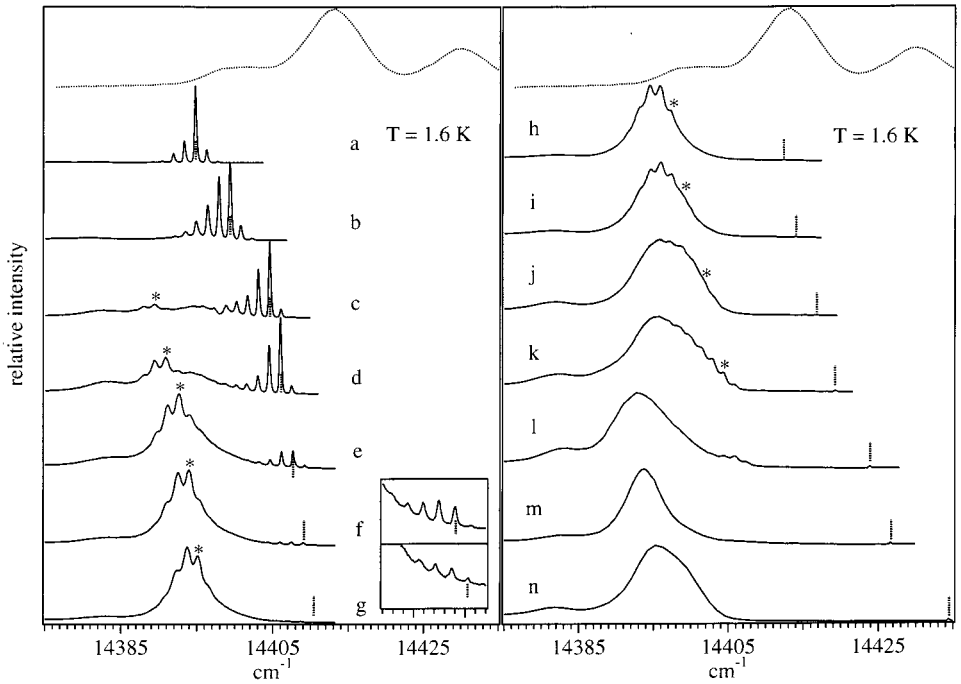

Figure 2. FLN spectra of $[Ru(bpy)_3][LiCr(ox)_3]$ as a function of the laser frequency $\tilde{\nu}_{ex}$ (····) in the region of the R lines at 1.6 K. The labels a−n refer to the laser frequencies marked by arrows in Figure 1. For the lines marked with an asterisk, $\tilde{\nu} = \tilde{\nu}_{ex} - 15.2$ cm^{-1}. (·····) Absorption spectrum in the region of the R lines of $[Ru(bpy)_3][LiCr(ox)_3]$ at 10 K.

This behavior is similar to the one found for $[Rh(bpy)_3][NaCr(ox)_3]ClO_4$ with all $[Cr(ox)_3]^{3-}$ chromophores on crystallographically equivalent sites:[1] It is indicative of resonant energy transfer within the R_1 line. For excitation at the low energy edge of the R_1 absorption, nearly a normal three-line spectrum is observed. But at higher excitation frequencies more lines appear both at higher and at lower energies with respect to the central (resonant) line, and there is a bias toward those lines at lower energies. The fwhm of $\sim$0.3 cm^{-1} of the sharp lines in the spectra a−d of Figure 2 is limited by the experimental resolution. The spacing between adjacent lines $D^L \approx 1.45$ cm^{-1}. In spectra c and d there is additional structured luminescence at lower energies with respect to the multiline pattern. This luminescence is due to an additional excitation into the low-energy edge of the inhomogeneously broadened R_2^L absorption that overlaps somewhat with the high-energy-edge of the R_1^L absorption. The ^2E splitting of site L can thus be determined as $D^L(^2E) = 15.2$ cm^{-1}. In the following, the nonresonant lines in the R_1^L region with an emission energy $\tilde{\nu} = \tilde{\nu}_{ex} - 15.2$ cm^{-1} are called correlated lines and are marked with an asterisk in the figures. With a value of 0.8 cm^{-1}, the fwhm of these lines is substantially larger than that of the resonant lines. This is due to a distribution of $D^L(^2E)$ around the above mean value and lifetime broadening of the R_2 state.[16]

Excitation into the region of the overlapping R_1^H and R_2^L lines results in luminescence in different spectral regions (Figure 2, spectra e−k). The region in the direct vicinity of the excitation frequency generally has a number of well-resolved sharp lines. These lines resemble the multiline spectra discussed above but now with spacings of approximately 1.55 cm^{-1}. They can be assigned to luminescence from the R_1^H state and the corresponding ground-state zero-field splitting D^H. Thus the $^4A_2$ zero-field splitting in site H is somewhat larger than the corresponding splitting in site L. In addition, there is comparatively strong luminescence at lower energies, which is assigned to the R_1^L luminescence getting its intensities either directly from R_2^L excitation or through energy transfer via R_1^H excitation. The R_1^L band shows a strong broad background with a multiline pattern superimposed. The fwhm of the lines of the R_1^L multiline structure is larger than those in the resonant region and is thus no longer limited by the experimental resolution. With increasing excitation frequency the ratio of the integrated luminescence $I(R_1^L)/I(R_1^H)$ increases dramatically, so that eventually hardly any luminescence is detected in the R_1^H region (Figure 2, spectra g−j).

Upon excitation into the R_2^H line of site H (Figure 2, spectra l−n) only nonresonant luminescence is obtained in both R_1 regions. The spectra show broad luminescence in the R_1^L region without any structure. Excitation into the low-energy edge of the R_2^H line results in weak luminescence in the R_1^H region which is still somewhat structured. Nevertheless, the fwhm of these lines is larger than those in the resonant multiline spectra (Figure 2, spectra e−g) discussed above. For excitation into the R_2^H line at even higher frequency, hardly any R_1^H luminescence is observed (Figure 2, spectrum n). The experimentally determined values of ground- and excited-state zero-field splittings for the two sites $D(^4A_2)$ and $D(^2E)$ are collected in Table 1.

3.3. Excitation Line Narrowing (ELN). In Figure 3, excitation line narrowing spectra measured at 1.5 K are given. The luminescence was detected selectively at different frequencies across the broad line luminescence. The detection frequency of spectrum a is at the energy of the low-energy shoulder attributed to a minority site. It basically consists of a three-line spectrum centered at the resonant line and broad unstructured bands at higher energies. For spectra b−d the luminescence was detected within the R_1^L band. The exact detection frequencies are marked with arrows. They show multiline structure in the R_1^L region. The region of the overlapping R_1^H and R_2^L bands is characterized by a broad background with a multiline pattern superimposed. The fwhm of lines of the R_1^H multiline structure is larger than the one in the resonant region. In addition, the R_2^H region shows a broad unstructured excitation band. Finally for spectrum e the detection frequency is tuned to the high-energy side of the R_1^H line. This results in three-line patterns around the resonant line as well as at the position of the corresponding R_2^H line. The fwhm is somewhat broader for the R_2^H region. The resulting $D^H(^2E)$ is 17.5 ± 0.5 cm^{-1} (see Table 1).

3.4. Time Dependence. For the time-resolved FLN spectra at 1.5 K shown in Figure 4a and b, the excitation took place at 14409.0 cm^{-1} and at 14419.6 cm^{-1}, that is at the low and the

TABLE 1: Spectroscopic Parameters of the Components of the ^2E Lines of the Two Sites in $[Ru(bpy)_3][LiCr(ox)_3]$[a]

	site L	site H
$D(^4A_2)$[b]	1.45 cm^{-1}	1.55 cm^{-1}
$D(^2E)$[b]	15.2 cm^{-1}	17.5 cm^{-1}
$\tilde{\nu}_a$[b]	14400.5 cm^{-1}	14413.0 cm^{-1}
Γ_{inh}[c]	9.1 ± 0.08 cm^{-1}	
$I(R_1/R_2)$[c]	1.85 ± 0.025	
I^H/I^L[d]	3.6 ± 0.14	
k_a/k_b[e]	2.8	

[a] $D(^4A_2)$ and $D(^2E)$ are the zero-field splittings of the ground- and the excited state, respectively, $\tilde{\nu}_a$ is the maximum of the absorption of the transition from the low energy component of the $^4A_2$ state, g_a, within the corresponding R_1 line, Γ_{inh} is the inhomogeneous line width, $I(R_1/R_2)$ is the intensity ratio of the R lines of one site, and I^H/I^L is the intensity ratio between the two sites. The terms k_a and k_b are the individual radiative decay rate constants of the R_1 line to the ground state components g_a and g_b [b] Observed from experiment. [c] Determined from fit (see text), assumed equal for the two sites. [d] Determined from fit (see text). [e] From ref 1.

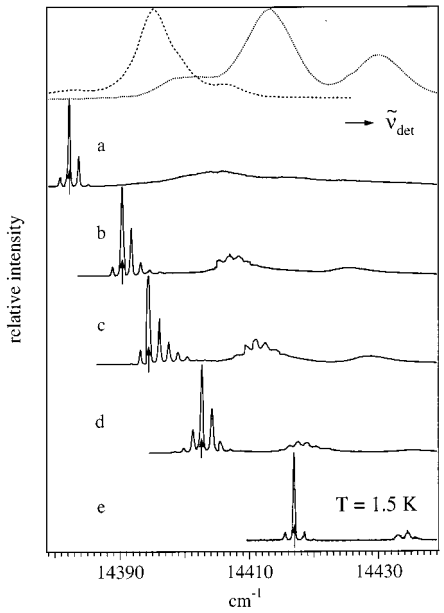

Figure 3. Resonant and nonresonant ELN spectra of $[Ru(bpy)_3][LiCr(ox)_3]$ at 1.5 K as a function of the detection frequency $\tilde{\nu}_{det}$ (marked by arrows) in the region of the R lines. (- - -) Luminescence spectrum in the region of the R lines upon nonselective excitation at 482 nm. (·····) Absorption spectrum in the region of the R lines of $[Ru(bpy)_3][LiCr(ox)_3]$ at 10 K.

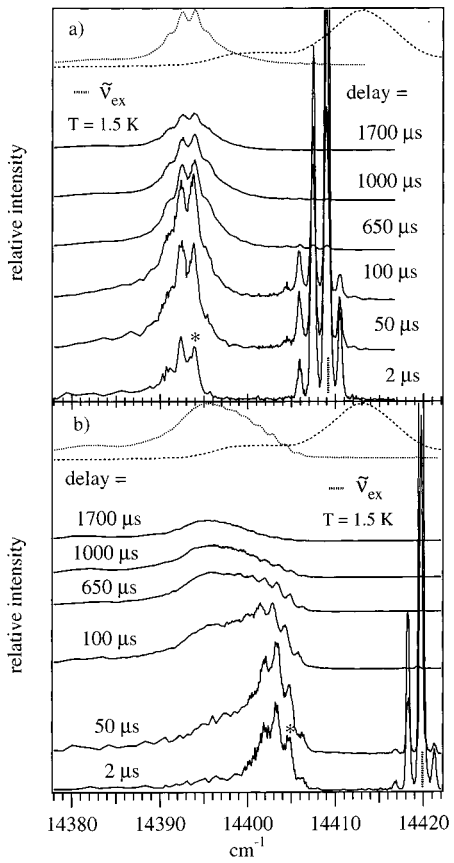

Figure 4. Time-resolved resonant and nonresonant FLN spectra of $[Ru(bpy)_3]$ $[LiCr(ox)_3]$ in the region of the R lines at 1.5 K. The delay times in μs are indicated in the figure. (a) $\tilde{\nu}_{ex} = 14409.0$ cm^{-1}; (b) $\tilde{\nu}_{ex} = 14419.6$ cm^{-1}.

high side of the overlapping R_1^H and R_2^L absorptions, respectively. The spectra were recorded at different delay times following the excitation pulse of 1−50 μs, and with detection time windows from 1 μs for short delays to 200 μs for longer delays.

Figures 4 a and b show the resulting spectra for delay times between 2 μs and 1700 μs. The corresponding steady-state FLN spectra are included for comparison. For both excitation frequencies luminescence is observed in two regions. Shortly after the pulse luminescence in the R_1^H region with a four line pattern and spacings of 1.55 cm^{-1} is dominant. In addition, there is weaker and poorly structured luminescence in the R_1^L region. At longer delay times more lines start to appear in the R_1^H region, but at the same time the integrated intensity of the R_1^H line decreases dramatically. This decrease is more rapid for the higher frequency excitation. The R_1^L luminescence has a broad background with a multiline pattern superimposed. The fwhm of the lines of the multiline structure in R_1^L region of 0.8 cm^{-1} is larger than those in the resonant regions at all delay times. In contrast to the R_1^H luminescence, the integrated intensity clearly increases with increasing delay times. Note that the R_1^L intensities of both the broad background as well as the superimposed multiline pattern increase in Figure 4a. The total intensity in the R_1^L region decreases only after very long delay times. For the higher frequency excitation (Figure 4b), the broad background luminescence grows asymmetrically with a tendency toward lower energies. Additionally, the R_1^H multiline structure vanishes for delay times of >100 μs.

4. Discussion

4.1. Absorption and Luminescence. The absorption spectrum of $[Ru(bpy)_3][LiCr(ox)_3]$ clearly indicates that there are at least two $[Cr(ox)_3]^{3-}$ sites: one site denoted H at higher energy, and a second site denoted L at lower energy with the R_1^H and the R_2^L bands having a large spectral overlap. From the crystal structure at room temperature only one $[Cr(ox)_3]^{3-}$ site is expected.[11] However, a preliminary X-ray diffraction study at 100 K gives an indication for a low-temperature phase transition.[23] Thus the three bands of the absorption spectrum of Figure 1 are made up of eight transitions, four for each site corresponding to the transitions from the two zero-field components of the $^4A_2$ state to the two zero-field components of the ^2E state. Each of these transitions is characterized by three parameters: its energy, its intensity, and by the width of its inhomogeneous distribution. Of course, a corresponding 24-parameter fit to the absorption spectrum of Figure 1 would be meaningless. However, the number of free parameters can be substantially reduced. From the FLN spectra, the zero-field splittings of the $^4A_2$ and the ^2E states for both sites are accurately known. Thus, only two of the eight energy parameters are required as free parameters in a fitting procedure. Likewise, it can safely be assumed that the inhomogeneous widths of the eight components are approximately equal. The eight intensity parameters can be reduced to two by assuming that the relative intensities of the R_1 to the R_2 lines are equal for the two sites. The second parameter is then simply the ratio between the intensities of the transitions of site H to the ones of site L.

In Figure 1 the resulting decomposition into site H and site L is illustrated. The corresponding fit parameters are given in Table 1. In the cubic space group $P2_13$, the unit cell has four equivalent lattice sites for the $[Cr(ox)_3]^{3-}$ chromophores. Lower symmetry due to a low-temperature phase transition can induce ratios of the chromophores of 3:1 or 2:2 for distortions along the trigonal or the tetragonal crystal axis, respectively. The experimental intensity ratio of 3.5:1 is closer to the former. Thus three of the four chromophores lose their C_3 site symmetry whereas the fourth chromophore retains its C_3 symmetry. The additional lowering of the site symmetry for three of the four chromophores can lead to larger oscillator strengths for the three chromophores as compared to the one on the C_3 site. The ratio of 3.5:1 thus indicates an increase of ∼20% for the oscillator strength of the more distorted chromophores. Furthermore, the decomposition shows that there are spectral overlaps of the different R lines, especially of the R_1^H and the R_2^L lines.

The fact that upon broad band excitation luminescence is observed predominantly from the R_1^L line shows that there is efficient energy transfer from site H to site L. The weak luminescence at 14406.0 cm^{-1} is due to partly quenched R_1^H luminescence. The weak line at 14382.6 cm^{-1}, which is at even lower energies than the R_1^L luminescence, is probably due to a minority site as it is not observed in absorption. Such low-energy luminescence from minority sites is often observed in concentrated systems where energy migration takes place. Energy transfer within the R lines of both sites is also indicated by the shifts of the band maxima of the R_1^H and R_1^L luminescence with respect to the corresponding band maxima in absorption.

4.2. Energy Transfer within the R_1^L and the R_1^H Line. FLN experiments allow to distinguish between different mechanisms for energy transfer. In the FLN experiments with direct laser excitation into the R_1^L line of $[Ru(bpy)_3][LiCr(ox)_3]$, multiline spectra with spacings of $D^L = 1.45$ cm^{-1} are obtained (Figure 2, spectra a−d). Multiline patterns are characteristic for energy selective and thus resonant energy transfer within the R_1^L line. A model for such resonant energy transfer has been presented previously.[1,16]

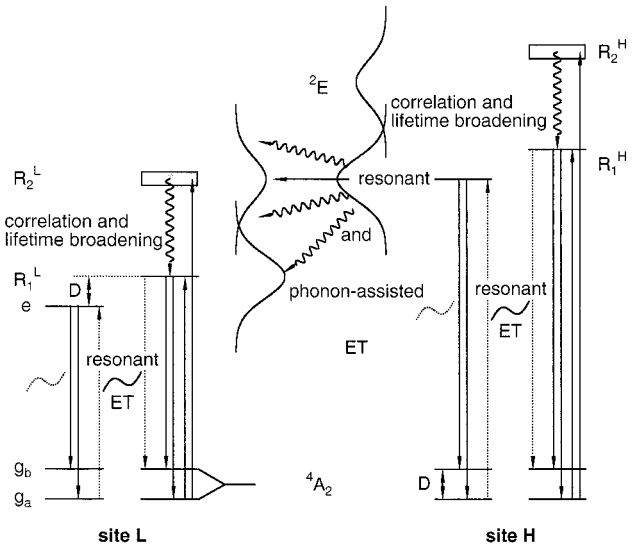

Figure 5. Schematic representation of the model for energy transfer processes of $[Cr(ox)_3]^{3-}$ in $[Ru(bpy)_3][LiCr(ox)_3]$. For simplicity, transitions originating from the thermally populated ground-state component have been omitted.

For selective excitation within the R_1^L transition and at liquid helium temperatures, only three energy levels of the octahedrally coordinated Cr^{3+} have to be considered (see Figure 5): the two zero-field components of the $^4A_2$ ground state (g_a and g_b) and the low-energy component of the ^2E state (e). With a splitting of 15.2 cm^{-1}, the high-energy component of the ^2E state is not populated at temperatures below 4.2 K. The requirements for the occurrence of multiline patterns are that the inhomogeneous line width Γ_{inh} of the transition is larger than the zero-field splitting of the ground state $D(^4A_2)$, which in turn is larger than the homogeneous line width Γ_{hom}. With two inhomogeneously broadened and overlapping transitions, two sets of molecules are excited at the laser frequency $\tilde{\nu}_{ex}$ within the inhomogeneous envelope: a set for which the transition $g_a \rightarrow e$ is resonant ($\tilde{\nu}_a = \tilde{\nu}_{ex}$) and a set for which the transition $g_b \rightarrow e$ is resonant ($\tilde{\nu}_b = \tilde{\nu}_{ex}$). The latter gives rise to hot bands. For simplicity the corresponding processes are not explicitly shown in Figure 5. As for the one-site systems discussed in refs 1 and 16, resonant energy transfer is possible within each of these subsets individually, but because each subset has two possible transitions and because Γ_{inh} is larger than D, additional resonant energy transfer processes are possible as, for instance, from the subset $\tilde{\nu}_a = \tilde{\nu}_{ex}$ to the subset at $\tilde{\nu}_a = \tilde{\nu}_{ex} - D$, for which the $g_a \rightarrow e$ transition is resonant with the $g_b \rightarrow e$ transition of the former, or from the subset at $\tilde{\nu}_b = \tilde{\nu}_{ex}$ to the subset at $\tilde{\nu}_b = \tilde{\nu}_{ex} + D$, for which the $g_b \rightarrow e$ transition is resonant with the $g_a \rightarrow e$ transition of the former. This results in a ladder spaced by D within the inhomogeneous distribution, with resonant energy transfer processes between spectral neighbors separated by $\pm D$.

Because the concentration of resonant $[Cr(ox)_3]^{3-}$ chromophores varies across the inhomogeneous distribution, the average distance between resonant chromophores, and therefore the probability for resonant energy transfer, varies too. Consequently, the structure of the multiline pattern depends strongly upon the excitation frequency. For excitation far into the low-energy tail, there are only a few resonant chromophores, and their distance from each other is so large that hardly any resonant energy transfer can occur. Thus almost a straightforward three line pattern like in diluted systems is observed. The most striking multiline pattern results for excitation at or near the center of the inhomogeneous distribution, where the concentration of resonant chromophores in subsets of spectral neighbors is comparatively large. Furthermore, at 1.6 K there is a bias for the resonant energy transfer toward the low-energy members of the resonant ladder. This is borne out by the spectra a−d of Figure 2, where more peaks at lower energies are observed than at higher energies with respect to the resonant line. Figure 6 shows the spectral region of the R_1^L line of the above series of spectra on an enlarged scale. In contrast to the previous report on the $[Rh(bpy)_3][NaCr(ox)_3]ClO_4$ system,[1] for $[Ru(bpy)_3][LiCr(ox)_3]$ the resonant line is always the most intense. Therefore, in the present system the efficiency of the resonant energy transfer within R_1^L must be lower than in the former system. This is not surprising because the $[Cr(ox)_3]^{3-}$ concentration of resonant subsets in the R_1^L line is smaller than in the R_1 line of $[Rh(bpy)_3][NaCr(ox)_3]ClO_4$ for which all $[Cr(ox)_3]^{3-}$ chromophores are crystallographically equivalent. Figure 6 also shows the calculated multiline patterns based on the model described in refs 1 and 16, using values of 10 cm^{-1} for Γ_{inh}, 1.45 cm^{-1} for $D(^4A_2)$ as observed experimentally for $[Ru(bpy)_3][LiCr(ox)_3]$, and transferring the values for the intrinsic decay rate constant k_r of 770 s^{-1} and the ratio $k_a/k_b = 2.8$ from the one-site system $[Rh(bpy)_3][NaCr(ox)_3]ClO_4$. The curves calculated using the pseudo-first-order rate constant for energy transfer by a dipole−dipole mechanism[1] $k_{et}^{L\prime}$ of 1.3×10^3 s^{-1} agree very well with the experimental spectra. This value has to be compared with the value of $k_{et}' = 10^4$ s^{-1} for the above-mentioned one-site system. The pseudo-first-order rate constant k_{et}' is defined as

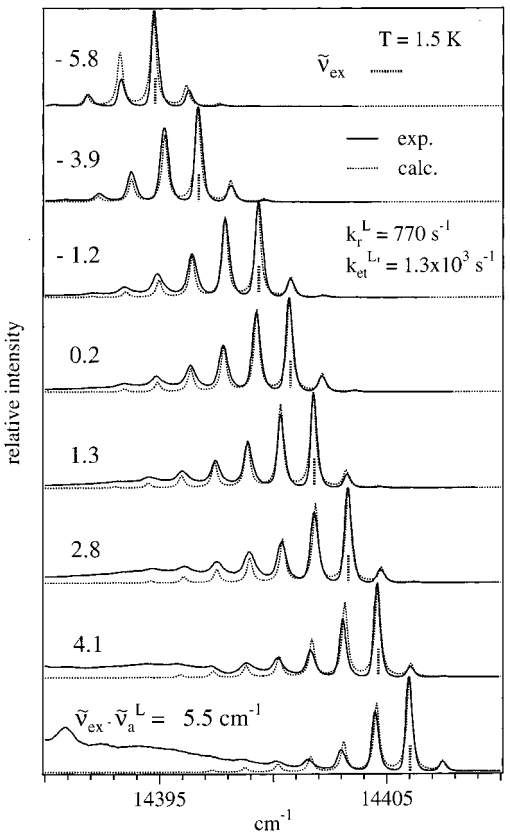

Figure 6. (—) Resonant FLN spectra of $[Ru(bpy)_3][LiCr(ox)_3]$ at 1.5 K as a function of the laser frequency $\tilde{\nu}_{ex}$(····) within the inhomogeneous line width of the R_1^L line. (·····) Simulated resonant FLN spectra using the parameters relevant for the $[Cr(ox)_3]^{3-}$ chromophore as given in the text and a pseudo-first-order rate constant $k_{et}' = 1.3 \times 10^3$ s^{-1}. Here, $\tilde{\nu}_{ex} - \tilde{\nu}_a^L$ is the energy difference between excitation frequency and the maximum of the absorption of the R_1 line of site L.

$$k_{et}' = k_{et} N_A^0 \qquad (1)$$

where k_{et} is the average bimolecular energy transfer rate constant and N_A^0 is the concentration of acceptors at the maximum of the inhomogeneous distribution. The value of k_{et} depends on oscillator strengths and spectral overlap integrals according to the Förster−Dexter equation[22,24,25] and N_A^0 depends on the total number of equivalent chromophores in the system and the ratio of homogeneous to inhomogeneous line widths. Assuming equal homogeneous line widths of 0.012 cm^{-1} for the two-site and the one-site systems,[1] N_A^0 for the two-site system is estimated to be approximately a factor of 8 smaller than for the one-site system. This estimation is based on inhomogeneous line width being a factor of 2 larger and the concentration of equivalent chromophores being a factor of 1/4 smaller due to the lower symmetry. As a result, $k_{et}^{L\prime}$ is expected to be $\sim 1/8\ k_{et}'$, and this agrees with the experimentally determined $k_{et}^{L\prime}$.

The intensity of the R_1^H absorption line is more than three times higher than the R_1^L line. Hence, the concentration of resonant subsets and therefore the efficiency of the energy transfer is expected to be higher within R_1^H as compared to R_1^L. Actually, this is what is being observed upon direct excitation into the R_1^H absorption. The FLN spectra e−g in Figure 2 show weak but distinct multiline patterns in the R_1^H region, mainly due to resonant energy transfer within the R_1^H line. In this case, the resonant line is not always the most intense because the resonant energy transfer down the ladder is sufficiently efficient.

4.4. Site-to-Site Energy Transfer. In Figure 5, all the possible energy transfer processes are shown schematically. Because energy transfer takes place from site H to site L, the spectra d−k in Figure 2, with excitation mainly into the R_1^H absorption band, show not only multiline patterns in the R_1^H region but also luminescence in the R_1^L region. The latter shows a broad background with a multiline pattern superimposed. The broad background indicates that there is efficient nonselective and thus phonon-assisted energy transfer, and the multiline structure could be due to either a partially resonant site-to-site energy transfer via the spectral overlap of the R_1^H and the R_2^L lines and subsequent relaxation to the R_1^L state, or to direct excitation into the R_2^L line or possibly a combination of the two. The time-resolved spectra shown in Figure 4a give an upper limit for the contribution of the direct excitation. In the spectrum recorded 2 μs after the pulse, a fraction of 28% of the total luminescence intensity is due to R_1^L luminescence. This luminescence is the upper limit due to direct excitation. The fact that at delay times up to 650 μs the multiline structure actually gains intensity in absolute terms can be due only to resonant site-to-site energy transfer.

An indication that even at the very short delay time of 2 μs resonant energy transfer has occurred is shown by the following. With the zero-field splitting of the ^2E state of site L, $D^L(^2E) = 15.2\ cm^{-1}$, the correlated line in Figure 4a must be the sharp line at 14393.8 cm^{-1}. This line is indicated with an asterisk. If the multiline pattern was due only to direct excitation into the R_2^L line, the intensity distribution should be similar to the resonant FLN spectrum of the R_1^L region. However, the corresponding resonant steady-state FLN spectrum, shown as spectrum a in Figure 2, is very different, with the resonant line being the most intense line, and comparatively weak satellites at $\pm D(^4A_2)$. Thus, in order for the satellite lines in the R_1^L region to become more intense than the central line, efficient resonant energy transfer within the R_1^H line must have occurred prior to the resonant transfer from R_1^H to R_2^L followed by nonradiative thermalization. This is further corroborated by the sequence of steady-state FLN spectra shown in Figure 2, where for irradiation into the R_1^H band the intensity of the correlated R_1^L line falls below that of the low-energy satellite line.

4.5. Lifetime Broadening and Correlation Losses. In general, the two R-lines are well correlated in crystalline Cr^{3+} materials,[20,21] that is, the distribution of the ^2E zero-field splitting $D(^2E)$ around some mean value is quite narrow. In the one-site system $[Rh(bpy)_3][NaCr(ox)_3]ClO_4$, a broadening of the R_1 line to 0.5 cm^{-1} on average was found for excitation via R_2.[16] This broadening has been assigned to lifetime broadening of the R_2 line, as also found in other Cr^{3+} systems,[21,26] rather than to correlation losses between the two R lines. However, an additional broadening due to correlation losses cannot be excluded a priori.

To explain the different line widths in our title compound $[Ru(bpy)_3][LiCr(ox)_3]$ for different irradiation wavelengths, the pathways of the various energy transfer processes have to be analyzed. For irradiation into R_1^L, the width of the sharp lines in the multiline patterns of $\sim$0.3 cm^{-1} corresponds to the experimental resolution. In reality this width is equal to twice the homogeneous line width, which for this compound is on the order of 0.012 cm^{-1}.[1] For irradiation into the R_2^L line, the line width in the R_1^L region increases to 0.8 cm^{-1}. Assuming good correlation between the two R lines, this is a measure of the lifetime broadening of the R_2^L line. In $[Ru(bpy)_3][LiCr(ox)_3]$ this lifetime broadening is slightly larger than in the one-site system. Irradiation into the R_2^H line results in an additional broadening of the lines in the R_1^L line pattern. This is due to the slight difference in the ground-state zero-field splittings of the two sites and the fact that resonant processes can occur within the R_1^H line prior to the site-to-site energy transfer as well as within the R_1^L line following site-to-site energy transfer. Upon excitation in the R_2^H line, the luminescence of the R_1^L line shows no structure anymore. Thus, by the time the energy gets to the R_1^L line, the fine structure is lost even if all energy transfer processes are predominantly resonant. Of course, some loss of fine structure can also be due to phonon-assisted processes to be discussed in the next section.

4.6. Phonon-Assisted Energy Transfer. In section 4.5 it was shown that there is a broadening of the lines in the multiline structure of the nonresonant FLN spectra due to lifetime broadening of the R_2 lines and the difference in ground-state zero-field splittings between the two sites. Nevertheless, these different sources of broadening of the lines in the multiline structure cannot explain the large background luminescence, for instance, in the FLN and ELN spectra shown in Figures 2 and 3, respectively. This background luminescence can be explained by phonon-assisted energy transfer within the R_1 lines and/or phonon-assisted site-to-site energy transfer. The broad background in the R_1^L region in Figure 4b, which increases with time and shifts toward lower energies, is typical for phonon-assisted energy transfer within the R_1^L line.[22] After excitation of a subset of $[Cr(ox)_3]^{3-}$ ions in the high energy wing of the inhomogeneous distribution, the broad luminescence begins to grow as the energy migrates toward lower energies into the maximum of the inhomogeneous distribution. It is difficult to observe whether there is also phonon-assisted energy transfer within the R_1^H line, because the R_1^H luminescence decreases very quickly due to site-to-site energy transfer (Figure 4b). It is, in any case, much slower than both the resonant process within R_1^H as well as site-to-site transfer. Thus, the comparatively intense background luminescence in the region of the R_1^L transition following excitation in the R_1^H line can be attributed to a phonon-assisted site-to-site energy transfer. Temperature dependent FLN experiments[18] show that overall the background

luminescence increases with increasing temperature, while the intensity of the resonant multiline pattern decreases. This is the signature for a phonon-assisted process becoming increasingly important at higher temperatures.

5. Conclusions

The $[Ru(bpy)_3][LiCr(ox)_3]$ system has two crystallographically non-equivalent $[Cr(ox)_3]^{3-}$ sites, and, as a consequence, a series of different dynamical processes can occur rather than just the one process observed in the system with only one site. In the two-site system resonant energy transfer takes place within both R_1 lines of the non-equivalent $[Cr(ox)_3]^{3-}$ chromophores. With the model for resonant energy transfer from ref 1, the energy transfer can be described quantitatively and the resulting pseudo-first-order energy transfer rate constant is found to be in agreement with the one found in the one-site system. In addition, energy transfer occurs from site to site. Steady-state and time-resolved FLN experiments show that this site-to-site energy transfer is, at least partially, a resonant process at liquid helium temperatures. This is due to good spectral overlap between the R_1 line of site H and the R_2 line of site L and a very good correlation between the R lines of the site L. Except for the energy transfer within the R_1^L line, phonon-assisted processes compete with the resonant processes even at 1.5 K.

Acknowledgment. We thank R. Pellaux and S. Decurtins for providing preliminary samples of the title compound. This work was financially supported by the Swiss National Science Foundation.

References and Notes

(1) von Arx, M. E.; Hauser, A.;. Riesen, H.; Pellaux, R.; Decurtins, S. *Phys. Rev. B* **1996** *54*, 15800.

(2) Hauser, A.; Riesen, H.; Pellaux, R.; Decurtins, S. *Chem. Phys. Lett.* **1996**, *2613*, 13.

(3) Imbusch, G. F.; Yen, W. M. In *Laser Spectroscopy and New Ideas*; Yen, W. M., Levenson, M. D., Eds.; Springer Series in Optical Sciences 54; Springer: Berlin, 1987; p 248.

(4) (a) Selzer, P. M.; Hamilton, D. S.; Yen, W. M. *Phys. Rev. Lett.* **1977**, *38*, 858. (b) Selzer, P. M.; Huber, D. L.; Barnett, B. B.; Yen, W. M. *Phys. Rev. B* **1978**, *17*, 4979.

(5) Holstein, T.; Lyo, S. K.; Orbach, R. *Phys. Rev. Lett.* **1976**, *36*, 891.

(6) Chu, S.; Gibbs, H. M.; McCall, S. L.; Passner, A. *Phys. Rev. Lett.* **1980**, *45*, 1715.

(7) Jessop, P. E.; Szabo, A. *Phys. Rev. Lett.* **1980**, *45*, 1712.

(8) Blasse, G. In *Energy Transfer Processes in Condensed Matter*; DiBartolo, B., Ed.; NATO ASI B114; Plenum Press: New York, 1984; p 251.

(9) Duval, E.; Monteil, A. In *Energy Transfer Processes in Condensed Matter*; DiBartolo, B., Ed.; NATO ASI B114; Plenum Press: New York, 1984; p 643.

(10) Wasiela, A.; Merle d'Aubigne, Y.; Bock, D. *J. Lumin.* **1986**, *36*, 11. Wasiela, A.; Merle d'Aubigne, Y.; Bock, D. *J. Lumin.* **1986**, *36*, 24.

(11) Schmalle, H. W.; Pellaux, R.; Decurtins, S., unpublished results.

(12) Sugano, S.; Tanabe, Y.; Kamimura, H. *Multiplets of Transition Metal Ions*, Pure and Applied Physics Vol. 33; Academic Press: New York, 1970.

(13) Schönherr, T.; Spanier, J.; Schmidtke, H. H. *J. Phys. Chem.* **1989**, *93*, 5959.

(14) Decurtins, S.; Schmalle, H. W.; Pellaux, R.; Schneuwly, P.; Hauser, A. *Inorg. Chem.* **1996**, *35*, 1451.

(15) Decurtins, S.; Schmalle, H. W.; Schneuwly, P.; Ensling, J.; Gütlich, P. *J. Am. Chem. Soc.* **1994**, *116*, 9521.

(16) von Arx, M. E.; Langford, V. S.; Oetliker, U.; Hauser, A. *J. Phys. Chem. A.* **2002**, *106*, 7099.

(17) von Arx, M. E.; van Pieterson, L.; Burattini, E.; Hauser, A.; Pellaux, R.; Decurtins, S. *J. Phys. Chem. A.* **2000**, *104*, 833.

(18) von Arx, M. E., unpublished results.

(19) Szabo, A. *Phys. Rev. Lett.* **1971**, *27*, 323.

(20) Riesen, H.; Krausz, E. *Comments Inorg. Chem.* **1993**, *14*, 323.

(21) Riesen, H *J. Lumin.* **1992**, *54*, 71.

(22) Henderson, B.; Imbusch, G. F. *Optical Spectroscopy of Inorganic Solids*; Clarendon Press: Oxford, 1989; p 469.

(23) Capelli, S. C., unpublished results.

(24) Förster, Th. *Ann. Physik* **1948**, *2*, 55.

(25) Dexter, D. L. *J. Chem. Phys.* **1953**, *21*, 836.

(26) Rives, J. E.; Meltzer, R. S. *Phys. Rev. B* **1977**, *16*, 1808.